



Deposited via The University of Leeds.

White Rose Research Online URL for this paper:

<https://eprints.whiterose.ac.uk/id/eprint/104275/>

Version: Accepted Version

---

**Article:**

Vivacqua, V, Ghadiri, M, Abdullah, AM et al. (2016) Analysis of partial electrocoalescence by Level-Set and finite element methods. *Chemical Engineering Research and Design*, 114. pp. 180-189. ISSN: 0263-8762

<https://doi.org/10.1016/j.cherd.2016.08.019>

---

© 2016, Elsevier. Licensed under the Creative Commons Attribution-NonCommercial-NoDerivatives 4.0 International <http://creativecommons.org/licenses/by-nc-nd/4.0/>

**Reuse**

Items deposited in White Rose Research Online are protected by copyright, with all rights reserved unless indicated otherwise. They may be downloaded and/or printed for private study, or other acts as permitted by national copyright laws. The publisher or other rights holders may allow further reproduction and re-use of the full text version. This is indicated by the licence information on the White Rose Research Online record for the item.

**Takedown**

If you consider content in White Rose Research Online to be in breach of UK law, please notify us by emailing [eprints@whiterose.ac.uk](mailto:eprints@whiterose.ac.uk) including the URL of the record and the reason for the withdrawal request.

# ANALYSIS OF PARTIAL ELECTROCOALESCENCE BY LEVEL-SET AND FINITE ELEMENT METHODS

V. Vivacqua<sup>a</sup>, M. Ghadiri<sup>b\*</sup>, A. M. Abdullah<sup>a</sup>, A. Hassanpour<sup>b</sup>, M. J. Al-Marri<sup>c</sup>, B. Azzopardi<sup>d</sup>, B. Hewakandamby<sup>d</sup>, B. Kermani<sup>e</sup>

<sup>a</sup> *Center for Advanced Materials, Qatar University, Doha 2713, Qatar*

<sup>b</sup> *Institute of Particle Science and Engineering, University of Leeds, Leeds LS2 9JT, UK*

<sup>c</sup> *Gas Processing Center, Qatar University, Doha 2713, Qatar*

<sup>d</sup> *Department of Chemical and Environmental Engineering, University of Nottingham, Nottingham NG7 2RD, UK*

<sup>e</sup> *Keytech, Camberley GU15 2BN, UK*

## Abstract

The coalescence of a water drop in a dielectric oil phase at a water layer interface in the presence of an electric field is simulated by solving the Navier-Stokes and charge conservation equations with the finite element method. The proprietary software Comsol Multiphysics is used for this purpose. The interface between the oil and water phases is tracked by implementing a Level Set approach. The sensitivity of the model with respect to some input parameters are reported. In particular, the calculations are sensitive to the size of the computational grid elements, interface thickness and re-initialisation parameter. The ratio between the volume of secondary droplets and the initial drop volume is calculated as a function of the initial drop size and compared with experiments available in the literature. A good quantitative agreement can be obtained if the parameters are suitably tuned. The model also predicts a strong role played by the water phase conductivity in the formation of progeny droplets.

**Keywords:** Electrocoalescence; Partial coalescence; Modelling; Level Set Equation; Computational Fluid Dynamics.

\*Corresponding author. Tel.: +44 113 343 2406; Fax: +44 113 343 2384.

E-mail address: m.ghadiri@leeds.ac.uk

## 1. Introduction

External electric fields are used in the oil industry to promote migration of droplets in the water-in-oil emulsions formed during the oil extraction process and to enhance their coalescence [1, 2]. In the presence of an electric field, the rate of film thinning between two coalescing droplets increases [1], but partial coalescence can occur if the field strength is too high [3-6]. The formation of small secondary droplets undermines the efficiency of the separation process; it would therefore be highly beneficial to understand the operating conditions that favour incomplete coalescence. It has recently been shown [5] that the ratio between the volume of the secondary droplet formed and the initial drop volume is strongly correlated with the product of the Weber and Ohnesorge numbers. According to the same authors, the volume of the secondary droplets decreases if pulse-DC fields are used: the incidence of partial coalescence almost vanishes in the frequency range between 1 and 100 Hz using square, sawtooth and sinusoidal waves [6].

Although the findings described above can have an important impact on the development of compact electrocoalescers, a mathematical description of the process is needed for the extrapolation of these results to more general cases and provide guidelines to select the best operating conditions under which the separation efficiency is enhanced. In general, modeling of two-phase electrohydrodynamic flows are usually based on the simultaneous solution of Navier-Stokes, Poisson and charge distribution equations (neglecting magnetic phenomena), coupled with a method to track the interface between the two fluids. Convection of free charge needs to be modelled for a leaky dielectric fluid with non-zero conductivity whenever the time scale for the flow is comparable to the electric relaxation time. In this respect, Ristenpart et al. [7] have shown that the extreme case of non-coalescence is most probably related to the mechanism of charge transfer through short-lived bridges between bouncing drops. This suggests that the time resolution of the electric field variation is essential to capture the phenomenon of partial coalescence.

The accurate modeling of moving interfaces is also extremely important and is an area currently under active investigation. Explicit approaches, such as boundary integral and front-tracking methods, track discrete points on the interface surface. The motion and deformation of droplets under the presence of an electric field [8-12] and electro-jetting due to Taylor's instability [13] have been reproduced using this type of techniques. However, their implementation is not straightforward as the addition of surface-marker points is usually needed in order to obtain sufficient interface

resolution when stretching, coalescence and pinching occur. On the other hand, implicit methods, such as Level Set, Phase Field or Volume of Fluid methods, handle topological changes easily by defining an auxiliary function to represent the interface. These methods have also been used extensively to model droplet motion, deformation and coalescence under the effect of an externally applied electric field [14-20]. Each implicit technique to represent the interface has its own advantages and drawbacks. The Level Set method [21], which is used in this paper, is relatively simple, represents the effect of surface tension slightly more accurately. These features are important to correctly simulate the shape of the droplet during pinching, as this subsequently determines the formation of a progeny drop [7]. Also, the Level Set method has already been applied to reproduce partial coalescence in the absence of the electric field [22, 23]. To the authors' knowledge, there few attempts reported in the literature at predicting the occurrence of incomplete coalescence in the presence of an electric field. Teigen *et al.* [23] modelled the process using a combination of level-set and ghost fluid methods, as described in detail in [24]. Suppression of partial coalescence was predicted for an intermediate value of the electric Bond number, reproducing qualitatively the trend of previous investigators [25]. However, the physics of charge relaxation was not considered, which has instead been included in this work. In another modelling study [26], an electrokinetic model was employed to reproduce the transition from complete to partial electrocoalescence at increasing conductivity, revealing the importance of considering the charge separation dynamics. The aim of this work is to provide a mathematical description of the phenomenon. For this purpose, a finite element approach combined with the Level-Set method is adopted to analyse the process of partial coalescence. The proprietary software Comsol Multiphysics (Comsol, Sweden) software has been used for this purpose. Most of the model equations presented in Section 2 are already implemented in Comsol (in particular, they are included in the Laminar Two-Phase Flow, Level-Set and Electric currents modules). The only user-defined function is the electric force which has been added as a volume force equal to the divergence of the Maxwell stress tensor.

## 2. Model

### 2.1 Model Equations

A Level Set approach is employed to track the boundaries between different phases. The evolution of the boundary is described by the equation [23]:

$$\frac{\partial \phi}{\partial t} + \mathbf{u} \nabla \phi = \lambda \nabla \cdot \left( \xi \nabla \phi - \phi (1 - \phi) \frac{\nabla \phi}{|\nabla \phi|} \right) \quad (1)$$

where  $\phi$  is a smooth step function which varies from 0 to 1 across different phase domains,  $\lambda$  is a re-initialization parameter, which gives stability to the solution and  $\xi$  is related to the thickness of the interface. The fluid velocity is denoted by  $\mathbf{u}$  (bold letters denote vectors). A preliminary step computes the distance between the initial interface and the nodes of the computational domain,  $D_{si}$ . The initial condition for the time dependent study is then calculated as:

$$\phi_0 = \frac{1}{1 + e^{\pm D_{si}/\xi}} \quad (2)$$

The positive sign is used in Eq.2 for points initially inside the interface, whereas the minus sign applies to the domain outside the interface. The interface is described by the Level Set  $\phi_0 = 0.5$ .

In the standard approach, the Level-Set function is initialised as a distance function [27]. Re-initialisation is however needed to keep the interface thickness constant, because, as the Level-Set function moves with the average fluid stream velocity, it does not remain an exact distance function due to numerical errors. Procedures for re-initialization as a distance function at intermediate time steps are therefore needed to keep the interphase thickness constant. In the approach used in Comsol, based on the Olsson and Kreiss' formulation [28], the intermediate step, necessary for keeping the interphase thickness constant, is combined with the level-set equation into a single equation, i.e. Eq. 1. The parameter  $\lambda$  determines the degree of numerical stabilisation. If it is too small, the interface thickness is not preserved. If too large, the interface moves incorrectly and convergence problems arise.

The parameter  $\xi$  determines the interface thickness through Eq.2. The interface is modelled as a diffuse boundary, so that the Level-Set variable is equal to 0.5 at the interface. The Level-Set variable exponentially decays to zero and increases to 1 inside and outside the drop, respectively.  $\xi$  determines the rapidity by which the Level-Set function varies with the distance of the domain points from the 0.5 Level-Set iso-contour. It could be shown that, as a first approximation, the interface thickness  $\cong 4\xi D$  where  $D$  is the drop size. This is obviously not a realistic value of interface thickness but real values cannot be used in simulations. As also shown in this work, convergence problems arise due to the abrupt change in composition across the two phases. The parameter  $\xi$  is regarded as an adjustable parameter in this work.

It should be noted that Eq. (1) is a non-conservative formulation of the Level Set equation, which attains convergence more easily but conserves the integral of the Level Set function only approximately, therefore introducing some errors in the calculations in terms of mass conservation. A conservative formulation can be obtained by applying the incompressibility condition  $\nabla \cdot \mathbf{u} = 0$  [28], so that Eq.1 becomes:

$$\frac{\partial \phi}{\partial t} + \nabla \cdot (\phi \mathbf{u}) = \lambda \nabla \cdot \left( \xi \nabla \phi - \phi(1 - \phi) \frac{\nabla \phi}{|\nabla \phi|} \right) \quad (1')$$

However, the solution of the above equation is characterised by convergence problems which and this makes it unsuitable for a broad testing of the model capabilities. The non-conservative formulation is therefore used in this paper in order to explore a larger number of cases.

Navier-Stokes and continuity equations are solved using average physical properties for the two phases:

$$\rho(\phi) \frac{\partial \mathbf{u}}{\partial t} + \rho(\phi) (\mathbf{u} \cdot \nabla) \mathbf{u} = -\nabla p + \nabla \cdot \left( \mu(\phi) (\nabla \mathbf{u} + \nabla \mathbf{u}^T) \right) + \mathbf{F}_\gamma + \mathbf{F}_E \quad (3)$$

$$\nabla \cdot \mathbf{u} = 0 \quad (4)$$

where  $\rho(\phi)$  and  $\mu(\phi)$  are functions of the Level Set function and differ from the pure liquids properties only in the narrow region close to the interface where  $\phi$  varies. In general, the properties of the two liquids are weighted according to the equation:

$$P(\phi) = P_1 + (P_2 - P_1)\phi \quad (5)$$

In eq. (3), forces due to surface tension and induced by the electric field are included. The force due to surface tension is calculated as derived in [29]:

$$\mathbf{F}_\gamma = \nabla \cdot \left( \gamma (\mathbf{I} - (\mathbf{n}\mathbf{n}^T)) \delta \right) \quad (6)$$

where  $\gamma$  is the surface tension coefficient,  $\mathbf{I}$  the identity matrix,  $\mathbf{n}$  the outward pointing interface normal vector and  $\delta$  a smooth approximation of the Dirac function which is non-zero only at the interface.  $\mathbf{n}$  and  $\delta$  are calculated as, respectively:

$$\mathbf{n} = \frac{\nabla \phi}{|\nabla \phi|} \Big|_{\phi=0.5} \quad (7)$$

$$\delta = 6|\nabla \phi| |\phi(1 - \phi)| \quad (8)$$

The electric force is calculated from the divergence of the Maxwell tensor:

$$\mathbf{F}_E = \nabla \cdot \left( \varepsilon(\phi) \mathbf{E} \mathbf{E}^T - \frac{1}{2} \varepsilon(\phi) (\mathbf{E} \cdot \mathbf{E}) \mathbf{I} \right) \quad (9)$$

where  $\varepsilon(\phi)$  is the average permittivity. The electric field  $\mathbf{E}$  is computed by satisfying the charge conservation equation:

$$\nabla \cdot \left( \sigma(\phi) \mathbf{E} + \varepsilon(\phi) \frac{\partial \mathbf{E}}{\partial t} \right) = 0 \quad (10)$$

where  $\sigma(\phi)$  is the average conductivity. With reference to the computational domain depicted in Figure 1a, the following boundary conditions have been applied in order to solve this set of equations: the upper boundary is kept at a fixed electric potential while the opposite one is earthed and no-slip conditions are prescribed for both boundaries; the domain is axisymmetric; slip conditions are considered on the right boundary ( $\mathbf{u} \cdot \mathbf{n} = 0$ ) as done in [22], as this allows significant reduction of the simulation domain.

## 2.2 Non-dimensionalisation

Before discussing the results obtained by this approach, it is worth performing a dimensional analysis to determine which dimensionless groups control the phenomenon in this case. For this purpose, we shall introduce a characteristic time and length equal to  $D\gamma/\mu$  and  $D$ , respectively, so that:

$$t^* = \frac{\mu t}{D\gamma} \quad \nabla^* = D \cdot \nabla \quad \mathbf{u}^* = \frac{\mathbf{u}}{\gamma/\mu} \quad p^* = \frac{p}{\rho(\gamma/\mu)^2} \quad (11)$$

where  $D$  is the drop diameter. For the sake simplicity, the Level Set, Navier-Stokes and charge conservation equations will be written dropping the dependence of the liquid properties on  $\phi$ , obtaining:

$$\frac{\partial \phi}{\partial t^*} + \mathbf{u}^* \cdot \nabla^* \phi = \left( \frac{\lambda \mu}{\gamma} \right) \nabla^* \cdot \left( \left( \frac{\xi}{D} \right) \nabla^* \phi - \phi (1 - \phi) \frac{\nabla^* \phi}{|\nabla^* \phi|} \right) \quad (12)$$

$$\frac{\partial \mathbf{u}^*}{\partial t^*} + (\mathbf{u}^* \cdot \nabla^*) \mathbf{u}^* = -\nabla^* p^* + Oh^2 \nabla^* \cdot (\nabla^* \mathbf{u}^* + \nabla^* \mathbf{u}^{*\top}) + \mathbf{F}_\gamma^* + \mathbf{F}_E^* \quad (13)$$

$$\mathbf{F}_\gamma^* = Oh^2 \nabla^* \cdot \left( (\mathbf{I} - (\mathbf{nn}^\top)) \delta \right) \quad (14)$$

$$\mathbf{F}_E^* = We_{el} Oh^2 \nabla^* \cdot \left( \mathbf{E}^* \mathbf{E}^{*\top} - \frac{1}{2} (\mathbf{E}^* \cdot \mathbf{E}^*) \mathbf{I} \right) \quad (15)$$

$$\nabla^* \cdot \left( \mathbf{E}^* + \left( \frac{\varepsilon/\sigma}{D\mu/\gamma} \right) \frac{\partial \mathbf{E}^*}{\partial t^*} \right) = 0 \quad (16)$$

Inspection of Eqs (12)-(16) reveals that the phenomenon is regulated by the Ohnesorge  $Oh = \frac{\mu}{\sqrt{\rho\gamma D}}$ , electrical Weber number  $We_{el} = \frac{\varepsilon E_0^2 D}{\gamma}$ , as well as the groups  $\left( \frac{\lambda \mu}{\gamma} \right)$ ,  $\left( \frac{\xi}{D} \right)$  and  $\left( \frac{\varepsilon/\sigma}{D\mu/\gamma} \right)$ . The groups  $\left( \frac{\lambda \mu}{\gamma} \right)$ ,  $\left( \frac{\xi}{D} \right)$  are associated with the Level Set method and need to be tuned to reproduce the process. The last group controls the movement of charge in the process. It compares the time of pumping of the droplet content into the water layer with the dielectric relaxation time of the fluid. If this group is

$\ll 1$ , then it is not necessary to consider the movement of charge and Eq. (16) simplifies to the Laplace equation. For crude oil, the dielectric relaxation time is usually in the range  $10^{-4}$ - $10^{-2}$  s [30] and the water droplets in the emulsion are usually smaller than  $10^{-4}$  m. Unless the oil is very viscous, this suggests that the charge movement should also be considered in the analysis. Another important result of non-dimensionalising the equations is provided by Eq. (15) which shows that the electrostatic effect is mainly regulated by the product  $We_{el}Oh^2$ , which could explain why the volume of secondary droplets formed over the initial drop size has previously been correlated with the product  $We_{el}Oh$  [5].

### 3. Results and Discussion

The properties of the two liquids correspond to the sunflower oil/water system investigated experimentally by Mousavichoubeh *et al.* [5] and are reported in Table 1. The interfacial tension is equal to  $25 \text{ mN mm}^{-1}$ . It was measured according to a technique based on the pendant drop method, using a contact-angle measuring instrument, EasyDrop from Kruss GmbH. No appreciable variation with time was observed during the measurement. The conductivity was measured using a conductivity meter, Model 470 from JENWAY Products Inc. The voltage applied between two electrodes was between 1 and 11 kV. The current was measured using an electrometer, Model 6514 from Keithley Instruments. The current–voltage relationship for sunflower followed Ohm’s law.

The computational domain is 2D axisymmetric and Figure 1a. In Figure 1b, a close-up of the domain near the interface is reported to show the quality of the mesh generated with  $h_{\max}/D=0.03$ , where  $h_{\max}$  is the max mesh element size, which corresponds to the level of mesh refinement used in most of the simulations shown in this paper. The effect of the mesh element size, interface thickness, re-initialisation parameter, initial drop size and water conductivity on the model calculations are discussed in the following sections. In a typical simulation, a quite small time increment is employed, about  $10^{-7}$  s at the start of the simulation. The time step then increases up to about  $10^{-4}$  s in approximately 50 time steps and remains almost constant thereafter. However, the time step should be smaller than about  $10^{-5}$  s at the lower value of surface thickness parameter investigated in this work.

#### 3.1 Effect of the mesh size and interface thickness parameter

In order to assess the effect of  $\xi$  and the mesh element size, the following case is analysed. The initial drop size is 1.196 mm and the electric field strength is  $373 \text{ V mm}^{-1}$ . Under these conditions,

partial coalescence occurs and the ratio between the volume of the secondary droplets formed and the initial drop volume,  $V_r$ , is equal to about 0.088, as measured by Mousavichoubeh *et al.* [3].

The calculated values of  $V_r$  are reported in Table 2. This ratio is calculated from the Level Set parameter by integration over the computational domain  $\Omega_{\text{drop}}$ , where the initial or secondary drops are present (i.e. excluding the water layer). Considering that inside the water phase  $\phi = 0$ ,  $V_r$  is therefore computed as:

$$V_r = \frac{\int_{\Omega_{\text{drop}}} (1 - \phi) d\Omega \Big|_{t_{\text{final}}}}{\int_{\Omega_{\text{drop}}} (1 - \phi) d\Omega \Big|_{t_0}} \quad (17)$$

for  $0 \leq \phi \leq 0.5$ ,

For all cases presented in this section, the re-initialization parameter  $\lambda$  is set equal to 1 m/s, which is comparable to the maximum fluid velocity in the system, and the drop is falling from an initial distance of 0.1 mm.

The results shown in Table 2 reveal that tuning of the interface thickness,  $\xi$ , is strictly connected to the level of mesh refinement, i.e.  $h_{\text{max}}/D$ . With  $\xi/D=0.03$  or  $0.05$ , the calculated volume of secondary droplets becomes invariant with the grid element size when this is sufficiently small. In this case the volume ratio of the secondary droplet to that of the initial drop is very close to the experimental value. However, the phenomenology described in the two simulations is different, and the results are compared in Figures 2 and 3. The interface is given by the loci where the Level-Set variable is equal to 0.5. The value of  $\xi/D=0.02$  does not produce realistic results and convergence fails in a number of cases of  $h_{\text{max}}/D$ . The behaviour observed experimentally is also reported in Figure 4. The numerical results obtained with  $\xi/D=0.03$  and  $h_{\text{max}}/D=0.03$  reproduce the experimental observations accurately, whereas with  $\xi/D=0.05$  and  $h_{\text{max}}/D=0.03$  a jet-like behavior is reproduced. The predicted volume ratio is, however, very close to the experimental value in both cases. For  $\xi/D=0.03$  and  $h_{\text{max}}/D=0.03$ , the model is able to correctly predict both the volume of secondary droplets formed as well as the kinetics of coalescence, i.e. with a good correspondence between experimental and simulation times. However, some very small droplets formed cannot be reproduced, as an excessive mesh refinement would be necessary. In this regard, in Figure 5 the variation of the Level-Set variable is shown at different simulation times for  $\xi/D=0.03$  and  $h_{\text{max}}/D=0.03$ . From the calculations, it appears therefore evident that additional secondary droplets are most likely to form.

Table 2 also reveals that decreasing the interface thickness excessively leads to convergence problems, and a solution is obtained only for  $\xi/D=0.02$  and  $h_{\text{max}}/D=0.03$ , which, however, provides

a largervalue of the secondary droplet volume formed as compared to the experiments. Decreasing further the grid element size to 0.02 causes non-convergence again, as  $\xi/D$  should usually be smaller than the maximum grid size. This requirement becomes more critical when  $\xi/D$  is small.

### 3.2 Effect of the re-initialisation parameter

In the previous section the re-initialisation parameter was set to 1 m/s. However, different values of  $\lambda$  can lead to different simulation outcomes. In particular, with a too small value of  $\lambda$  the interface thickness does not remain constant during the simulation time. On the other hand, if  $\lambda$  is too large convergence becomes difficult. This means that  $\lambda$  should be optimized for a given application. A guideline to select an initial value of lambda is to set it equal to the maximum fluid velocity in the system and then follow an optimisation procedure. The values of  $\lambda$  used in this section are comparable to the calculated maximum fluid velocity in the system, but it has been considered as an adjustable variable in this work.

The volume ratio of the secondary droplet formed is shown in Figure 6 as a function of the re-initialisation parameter for  $D=1.196$  mm,  $\xi/D=0.03$  and  $h_{\max}/D=0.03$ . The progeny droplet volume remains almost constant for a wide range of values of  $\lambda$ , namely between 0.4 and 1.4 m/s, whereas it increases rapidly as  $\lambda$  is reduced below 0.4 m/s. At values of  $\lambda > 1.4$  m/s, convergence is not obtained. The fact that the calculations only vary slightly within a range of  $\lambda$  can be an indication of the possibility to apply a single value of  $\lambda$  to reproduce experiments with different operating conditions. This point is addressed in the next session, where the model is used to fit experimental data obtained with different initial drop size.

### 3.3 Variation of the model parameters with droplet size

The experimental measurements of  $V_r$  as a function of the initial droplet size for the system with properties reported in Table 1 [3] are shown in Figure 6. The numerical calculations obtained from the solution of the model equations are also reported in the same graph for comparison. The values of the model parameters used for each initial droplet size, namely  $\lambda$  and  $\xi/D$ , are given in Table 3. Using slightly different values of  $\lambda$  (0.5-0.6 m/s) and  $\xi/D$  (0.02-0.03), it is possible to reproduce approximately the trend of  $V_r$  versus  $D$ , apart from the smallest initial drop size, where under-damped oscillations do not readily occur, as it is shown by Vivacqua *et al.* [31]. The increasing/decreasing trend provided by the model calculations is also due to the fact the values of the interface thickness and re-initialisation parameters are different. This is due to convergence problems at certain values of these parameters, which prevented from using exactly the same values in all cases. It should be noted that

a more accurate optimization of the parameters could be carried out to fit the experimental data more closely; the results in Figure 7 are shown to demonstrate the capabilities of the model to replicate some aspects of the process using almost constant values of the parameters. However, this attempt fails while trying to reproduce the coalescence behaviour of the droplet with 0.576 mm initial size. It should be observed that a transition from partial to complete coalescence is expected by progressively decreasing the initial drop size. Below a certain value of the droplet size coalescence should become complete, as the deformation and necking tendency induced by the electric field decreases while the pumping action of surface tension is enhanced. However this does not occur experimentally when the initial drop size is 0.576 mm. For this diameter, either full coalescence or non-coalescence could be simulated only, with the two different behaviours obtained with different values of the initial falling distance, 0.08 and 0.1, mm respectively. This is perhaps due to the fact that starting the simulation from a position closer to the interface, determines a smaller contact angle at the intersection of the two Taylor cones formed between the drop and layer surfaces. In this respect, it has been shown that the phenomenology changes from full coalescence to bouncing or non-coalescence beyond a certain value of this contact angle [7]. Also, bouncing may be favoured by a larger kinetic energy of the droplet approaching the interface. The two different simulated behaviours are presented in Figure 8, where a complete coalescence and a bouncing/partial coalescence are shown in Figure 8 (a&b), respectively. Pillai et al. [26] also predicted that a larger initial separation distance demotes complete coalescence..

### 3.4 Effect of water conductivity

The water phase is always associated with the presence of dissolved salts, and this is particularly true during offshore oil extraction. Most of the existing literature, however, focuses on the electrocoalescence of distilled water droplets. Water salinity affects the electrical conductivity of the water phase, but its effect on the electrocoalescence process has not been reported in the literature extensively. In Figure 9,  $V_r$  is plotted as a function of  $\sigma_w$  for  $D=1.196$  mm,  $\lambda=1$  m/s,  $\xi/D = 0.03$  and  $h_{max}/D=0.03$ . Surprisingly, according to the model predictions, a clear maximum is found at  $\sigma \approx 10^{-3}$  S/m. Above about  $\sigma_w \approx 2 \times 10^{-2}$  S/m  $V_r$  becomes practically independent of  $\sigma$ . In Figure 10, the time evolution of the drop-interface coalescence event is reported for  $\sigma_w = 10^{-3}$  S/m, revealing a jet-like behavior. The dynamics of coalescence at  $\sigma_w = 2 \times 10^{-2}$  S/m is shown in Figure 11. In line with the trend of data in Figure 9, the pattern becomes similar to what previously illustrated in Figure 4 for  $\sigma_w \approx 5.49 \times 10^{-6}$  S/m.

A possible rationale for this finding can stem from the fact that varying conductivity can produce different contrasting effects.

- 1) As the conductivity is increased, the dipole moment induced onto the drop increases. This brings about a higher deformation of the drop, which tends to increase the volume of the secondary drop ejected. However, this effect becomes negligible beyond a certain value of conductivity [8].
- 2) With the increasing conductivity, the dimensionless group  $\left(\frac{\epsilon/\sigma}{D\mu/\gamma}\right)$  decreases and the movement of charges becomes faster. Accordingly, the charges on the droplet surface close to the interface will tend to leak quickly into the water layer and a strong electrostatic repulsion ensues from the unbalanced charge on the opposite surface of the drop.
- 3) On the other hand, a higher polarization determines a stronger clamping force between the drop and the interface and larger current flows into the water bulk. It has been demonstrated that convective charge transfer plays an important role in the electrohydrodynamics of the process [32].

In the light of the above considerations, it is likely that the mechanism of charge transfer plays a key role in the secondary droplet formation. Further evidence is shown in Figure 12 where the maximum value of the secondary droplet volume formed corresponds to the highest value of space charge density in the region of coalescence.

Hamlin *et al.* [32] report the existence of a critical ionic conductivity that governs the response of a small charged droplet contacting a larger, oppositely charged droplet. Below the critical conductivity, the droplets partially coalesce; above the critical conductivity, the droplets bounce off one another. However, in Figure 2 of their work, the experimental data are quite scattered and the ratio of the secondary droplet size over the initial drop size may have a maximum with conductivity at low values of field strength. Also, in Figure 12 it is shown that the space charge becomes almost constant with  $\sigma$  beyond a certain value of conductivity. This is in qualitative agreement with Hamlin *et al.* [32]. The bouncing behaviour could not be reproduced for our system for the range of conductivity investigated, but the phenomenon also probably depends on the initial drop-interface separation distance. However, the predicted behaviour needs to be confirmed by further experimental work and this will constitute the basis for future work.

## Conclusions

The partial coalescence of water droplets in dielectric oils in the presence of an electric field has been analysed by the use of the Level-Set Method to describe the interface. It makes use of the Level Set approach to describe the interface. The effects of the mesh size, interface thickness, re-

initialisation parameter, drop size and water conductivity have been assessed. Non-dimensionalisation of the model equations has shown the importance of charge transfer mechanisms and also suggested that the phenomenon is mainly regulated by a combination of the Ohnesorge and electrical Weber numbers, as found experimentally in previous work [5].

The model proved to be capable of reproducing some phenomena observed experimentally. A satisfactory quantitative agreement can be achieved by the right selection of the model parameters and mesh element size. The occurrence of non-coalescence can also be reproduced, although it was predicted under conditions which do not display this behavior experimentally. The model also predicts an important role played by the water conductivity, which needs experimental validation.

The approach proposed can therefore be used for quantitative predictions of electrohydrodynamic phenomena, but the need for tuning the adjustable parameters is obviously a non-desirable feature. However, tuning these parameters does not require extensive work and a future aim is to verify whether the same values of the parameters can be used to predict a broader range of operating conditions, including more complex polydisperse water-in-oil systems. Also, the use of parameters can in principle be avoided by resorting to the approach described by Osher & Fedkiw's [27] which will be considered in future work.

This study constitutes the basis for the development of a reliable mathematical description which can be used for the design of a compact and efficient electrocoalescers, in order to provide useful guidelines for the selection of the most suitable electric field conditions to minimise the occurrence of partial coalescence.

## **Acknowledgement**

This work was made possible by NPRP grant #5-366-2-143 from the Qatar National Research Fund (A Member of The Qatar Foundation). The statements made herein are solely the responsibility of the authors.

## References

- 1) Mhatre, S., Vivacqua, V., Ghadiri, M., Abdullah, A.M., Al-Marri, M.J., Hassanpour, A., Hewakandamby, B., Azzopardi, B. and Kermani B., (2015). Electrostatic phase separation: A review, *Chem Eng Res Des*, 96, 177-195.
- 2) Vivacqua V., Mhatre S., Ghadiri M., Abdullah A. M., Hassanpour A., Al-Marri M. J., Azzopardi B., Hewakandamby B. and Kermani B., (2015). Electrocoalescence of water drop trains in oil under constant and pulsatile electric fields, *Chem Eng Res Des*, doi:10.1016/j.cherd.2015.10.006.
- 3) Aryafar H. and Kavehpour H.P. (2009). Electrocoalescence: Effects of DC electric fields on coalescence of drops at planar interfaces, *Langmuir* 25 (21), 12460–12465.
- 4) Mousavichoubeh M., Ghadiri M. and Shariaty-Niassar M., (2011a). Electro-coalescence of an aqueous droplet at an oil–water interface, *Chem Eng Process*, 50, 338-344.
- 5) Mousavichoubeh M., Shariaty-Niassar M. and Ghadiri M., (2011b). The effect of interfacial tension on secondary drop formation in electrocoalescence of water droplets in oil, *Chem Eng Sci*, 66, 5330–5337.
- 6) Mousavi S.H., Ghadiri M. and Buckley M., (2014). Electro-coalescence of water drops in oils under pulsatile electric fields, *Chem Eng Sci*, 120, 130 - 142.
- 7) Ristenpart W. D., Bird J. C., Belmonte A., Dollar F. and Stone H. A., (2009). Non-coalescence of oppositely charged drops, *Nature*, 461, 377-380.
- 8) Baygents, J.C., Rivette, N.J., Stone, H.A., (1998). Electrohydrodynamic deformation and interaction of drop pairs, *J. Fluid Mech.*, 368, 359–375.
- 9) Feng, J.Q., Scott, T.C., (1996). A computational analysis of electrohydrodynamics of a leaky dielectric drop in an electric field. *Model. Soft Matter* 141, 1–26.
- 10) Fernández, A., Tryggvason, G., Che, J., Ceccio, S.L., (2005). The effects of electrostatic forces on the distribution of drops in a channel flow: two-dimensional oblate drops. *Phys. Fluid* 17, 1–15.
- 11) Fernández, A., (2008). Response of an emulsion of leaky dielectric drops immersed in a simple shear flow: drops less conductive than the suspending fluid. *Phys. Fluid* 20, 043304-043304-18.
- 12) Hua, J.-S., Lim, L.-K., Wang, C.-H., (2008). Numerical simulation of deformation/ motion of a droplet suspended in viscous liquids under influence of steady electric field. *Phys. Fluid* 20, 11302–11317.
- 13) Collins, R.T., Jones, J.J., Harris, M.T., Basaran, O.A., (2008). Electrohydrodynamic tip streaming and emission of charged drops from liquid cones. *Nat. Phys.* 2, 149–154.

- 14) Singh, P., Aubry, N., (2007). Transport and deformation of droplets in a micro device using dielectrophoresis. *Electrophoresis*, 28, 644–657.
- 15) Teigen, K.E., Munkejord, S.T., (2009). Sharp-interface simulations of drop deformation in electric fields. *IEEE Trans. Dielectr. Electr. Insulat.*, 16, 475–482.
- 16) Teigen, K.E., Munkejord, S.T., (2010). Influence of surfactant on drop deformation in an electric field, *Phys. Fluid*, 22, 112104-1-10.
- 17) Mahlmann, S., Papageorgiou, D.T., (2011). Numerical study of electric field effects on the deformation of two-dimensional liquid drops in simple shear flow at arbitrary Reynolds number, *J. Fluid Mech.*, 626, 367–393.
- 18) López-Herrera, J.M., Popinet, S., Herrada, M.A., (2011). A charge-conservative approach for simulating electrohydrodynamic two-phase flows using volume-of-fluid, *J. Comput. Phys.*, 230, 1939–1955.
- 19) Tomar, G., Gerlach, D., Biswas, G., Alleborn, N., Sharma, A., Durst, F., Welch, S.W.J., Delgado, A., (2007). Two-phase electrohydrodynamic simulations using a volume-of-fluid approach, *J. Comput. Phys.*, 227, 1267–1285.
- 20) Lin, Y., Skjetne, P., Carlson, A. (2012). A phase field model for multiphase electrohydrodynamic flow. *Int. J. of Multiphase Flow*, 45, 1-11.
- 21) Sethian, James A. (1999). *Level Set Methods and Fast Marching Methods: Evolving Interfaces in Computational Geometry, Fluid Mechanics, Computer Vision, and Materials Science*. Cambridge University Press. ISBN 0-521-64557-3.
- 22) Ray B., Biswas G. and Sharma, A. (2010). Generation of secondary droplets in coalescence of a drop at a liquid–liquid interface. *J. Fluid Mech.*, 655, 72-104.
- 23) Teigen K. E., Munkejord S. T. and Bjørklund, E. A computational study of the coalescence process between a drop and an interface in an electric field. In: *Proceedings of 6th International Conference on CFD in the Oil & Gas, Metallurgical and Process Industries*, Norway, 2008.
- 24) Bjørklund, E. (2009). The level-set method applied to droplet dynamics in the presence of an electric field. *Comput. Fluids*, 38 (2), 358 - 369.
- 25) Allan R. S. and Mason S. G., (1961). Effects of electric fields on coalescence in liquid+liquid systems. *Trans. Faraday Soc.*, 57, 2027–2040.
- 26) Pillai R., Berry J. D., Harvie D. J. E., Davidson M. R. Electrophoretic effects on satellite droplet formation during electrocoalescence of microdrops. In: *11th International Conference on CFD in the Minerals and Process Industries CSIRO*, Melbourne, Australia, 2015.

- 27) Osher, S. and Fedkiw, R. Level set methods and dynamic implicit surfaces, Springer, London, 2003.
- 28) Olsson E. and Kreiss G., (2005). A Conservative Level Set Method for Two Phase Flow, *J. Comput. Phys.*, 210, 225–246.
- 29) Lafaurie B., Nardone C., Scardovelli R., Zaleski S. and Zanetti G., (1994). Modelling Merging and Fragmentation in Multiphase Flows with SURFER, *J. Comput. Phys.*, 113 (1), 134–147.
- 30) Lundgaard, L. E., Berg, G., Ingebrigtsen, S. and Atten, P. Fundamental aspects of electrocoalescence. In: J. Sjöblom (Ed.), *Emulsions and Emulsion Stability*, 2nd edition, Marcel Dekker, 2006.
- 31) Vivacqua V., Ghadiri M., Abdullah A. M., Hassanpour A., Al-Marri M. J., Azzopardi B., Hewakandamby B. and Kermani B., (2016). Linear dynamics modelling of electrocoalescence, submitted to *Chem Eng Res Des*.
- 32) Hamlin B. S., Creasey J. C. and Ristenpart W. D., (2012). Electrically tunable partial coalescence of oppositely charged drops. *Phys Rev Lett*, 109(9), 094501.

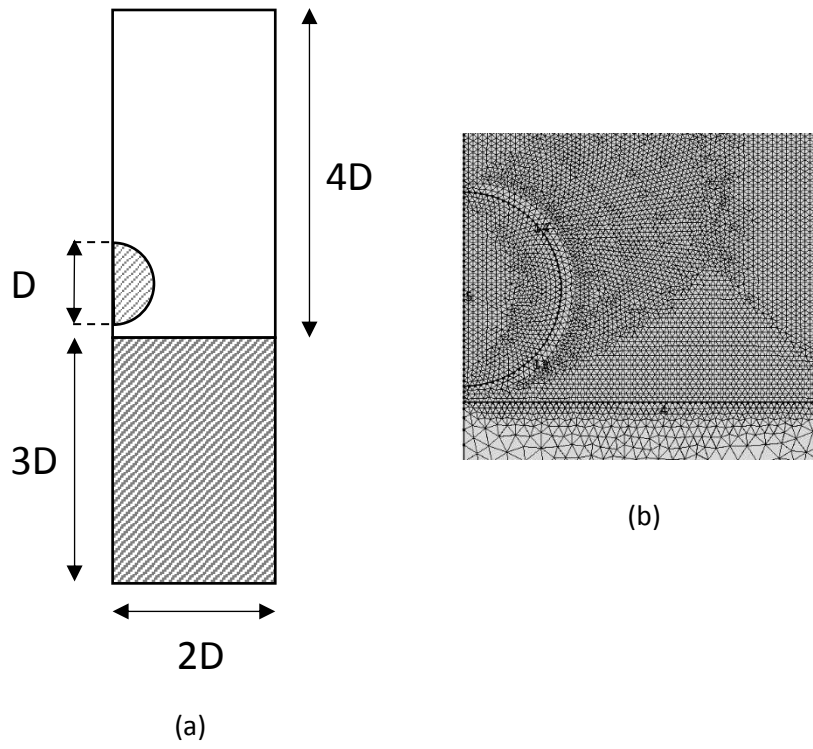


**Figure 1:** (a) Sketch of the simulation domain. (b) Close-up of the mesh for  $h_{\max}/D=0.03$ .

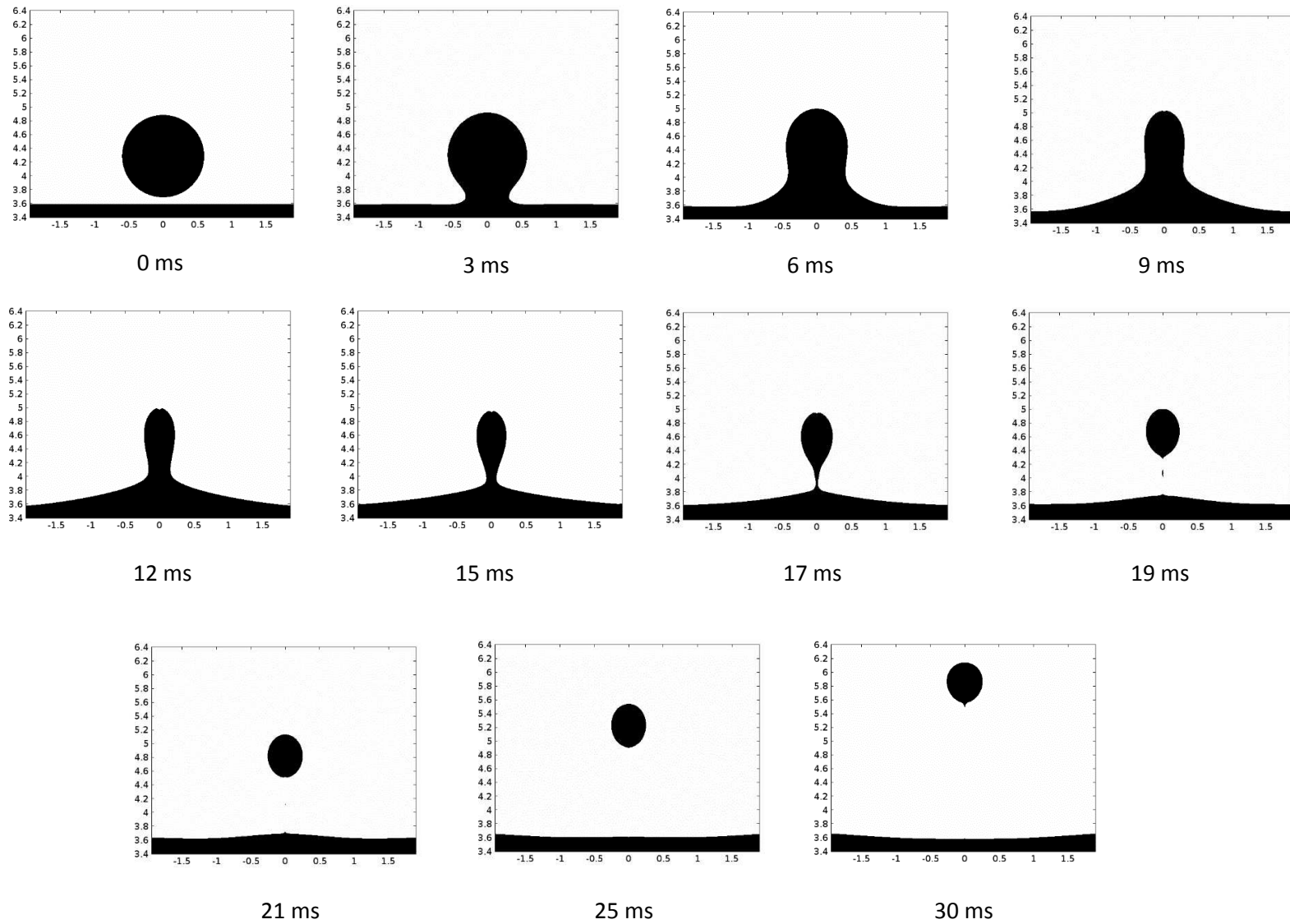


**Figure 2:** Time evolution of drop-interface coalescence:  $\xi/D=0.03$ ,  $h_{\max}/D=0.03$ ,  $\lambda=1 \text{ m s}^{-1}$ ,  $D = 1.196 \text{ mm}$ ,  $\sigma_w = 5.49 \cdot 10^{-6} \text{ S/m}$ .

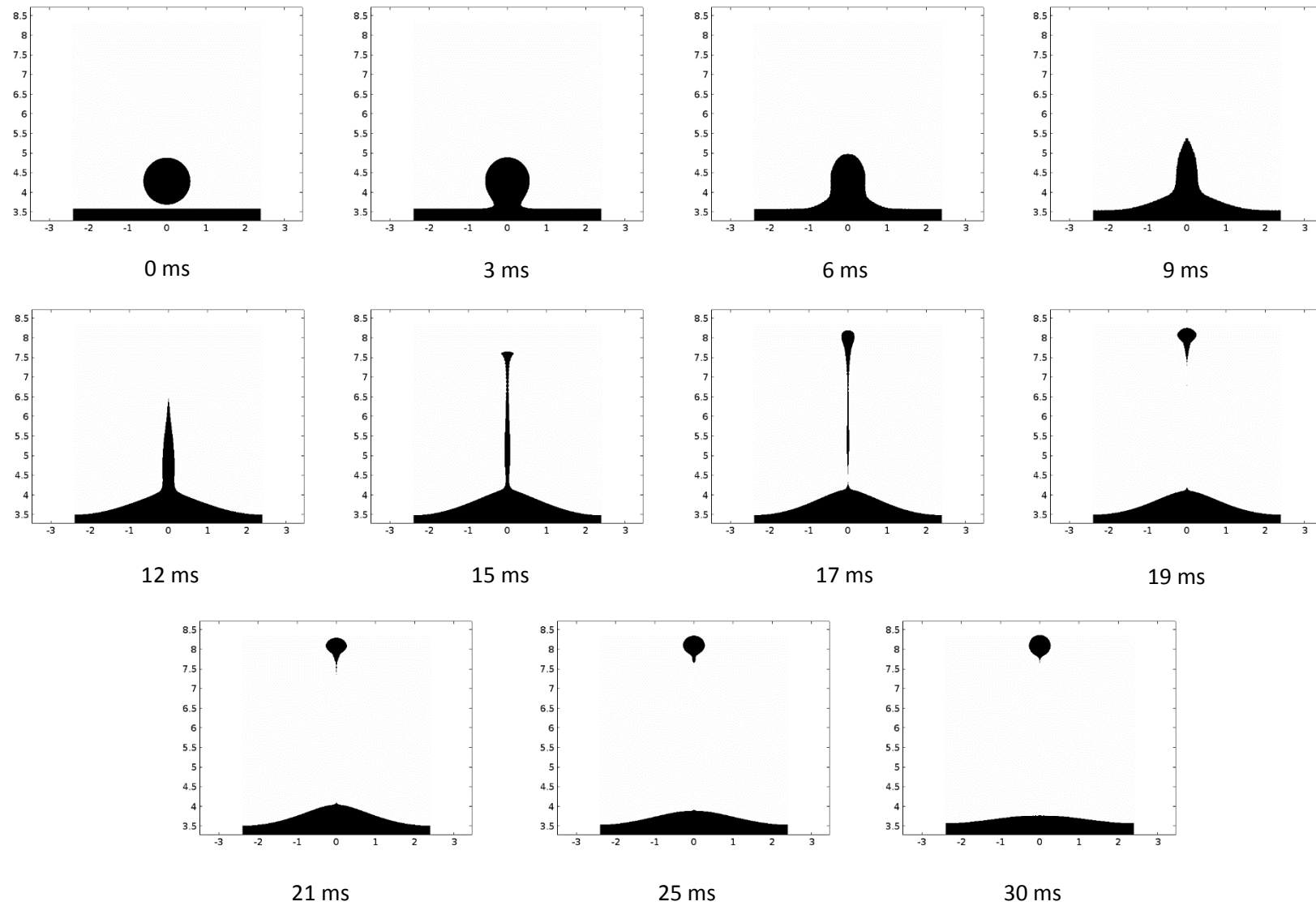


**Figure 3:** Time evolution of drop-interface coalescence:  $\xi/D=0.05$ ,  $h_{\max}/D=0.03$ ,  $\lambda=1 \text{ m s}^{-1}$ ,  $D = 1.196 \text{ mm}$ ,  $\sigma_w = 5.49 \cdot 10^{-6} \text{ S/m}$ .

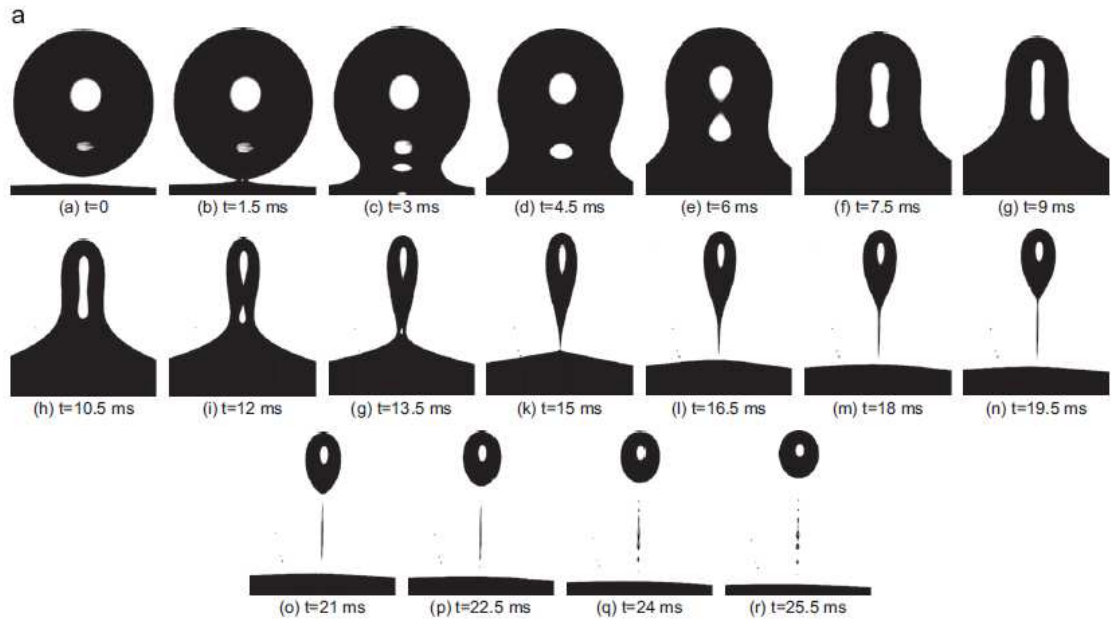


**Figure 4:** Partial coalescence of 1.926 mm drop at a water layer interface under  $373 \text{ kV mm}^{-1}$  electric field (adapted from Mousavichoubeh *et al.*, 2011b).

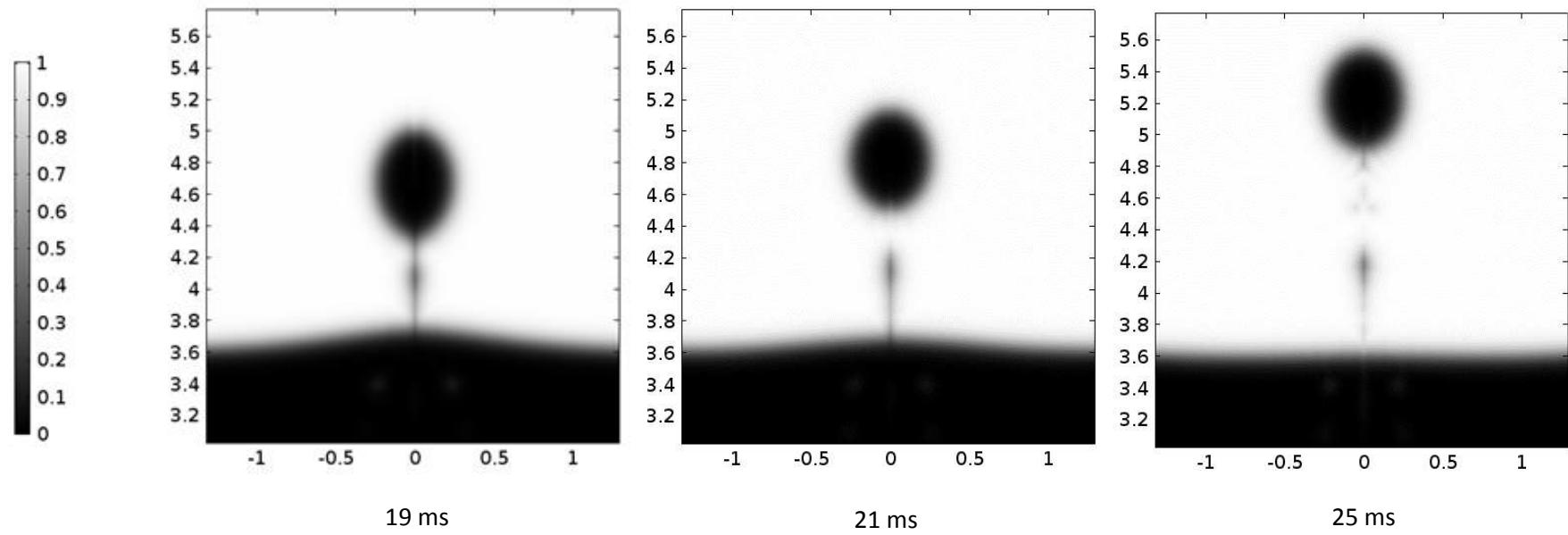


**Figure 5:** Level-Set plot at different simulation times:  $\xi/D=0.03$ ,  $h_{\max}/D=0.03$ ,  $\lambda=1 \text{ m s}^{-1}$ ,  $D = 1.196 \text{ mm}$ ,  $\sigma_w = 5.49 \cdot 10^{-6} \text{ S/m}$ .

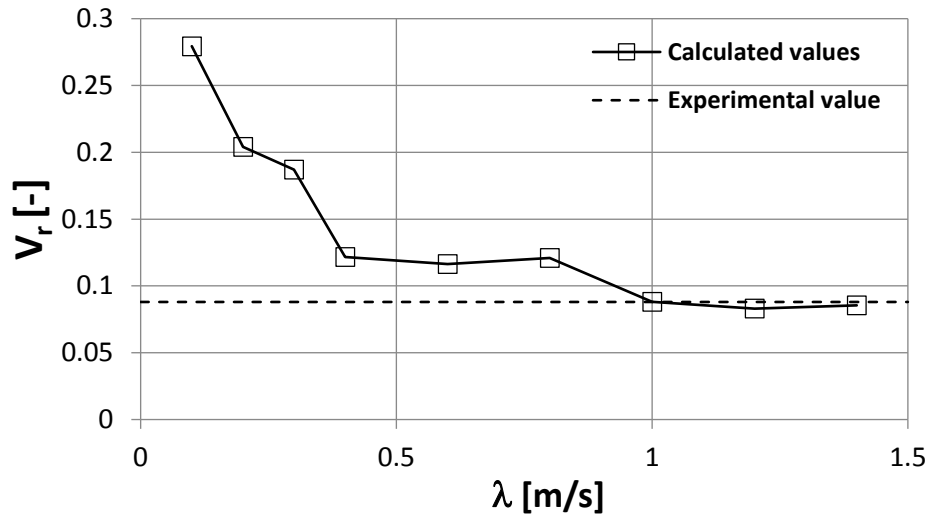


**Figure 6:** Effect of the re-initialization parameter on the calculated volume of secondary droplet formed with  $D=1.196$  mm properties reported in Table 2.

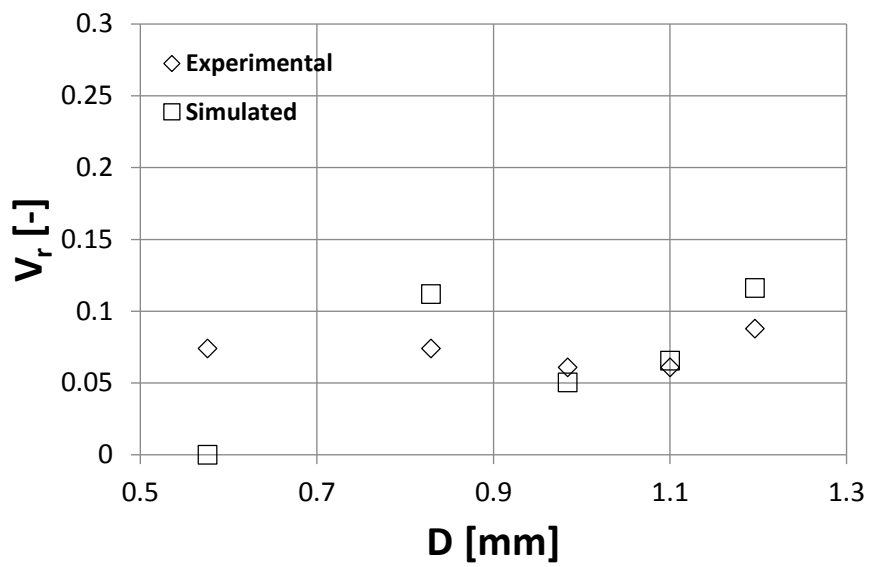
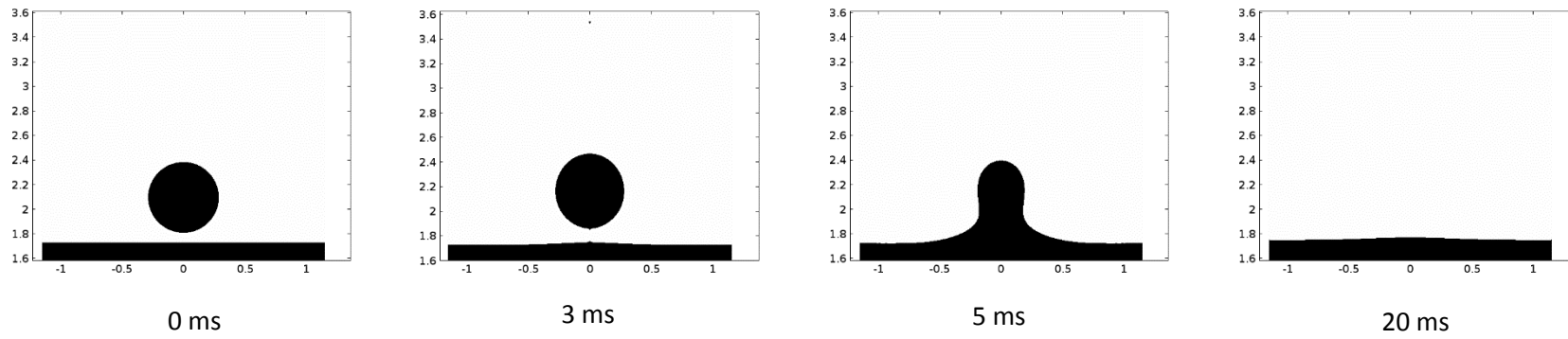
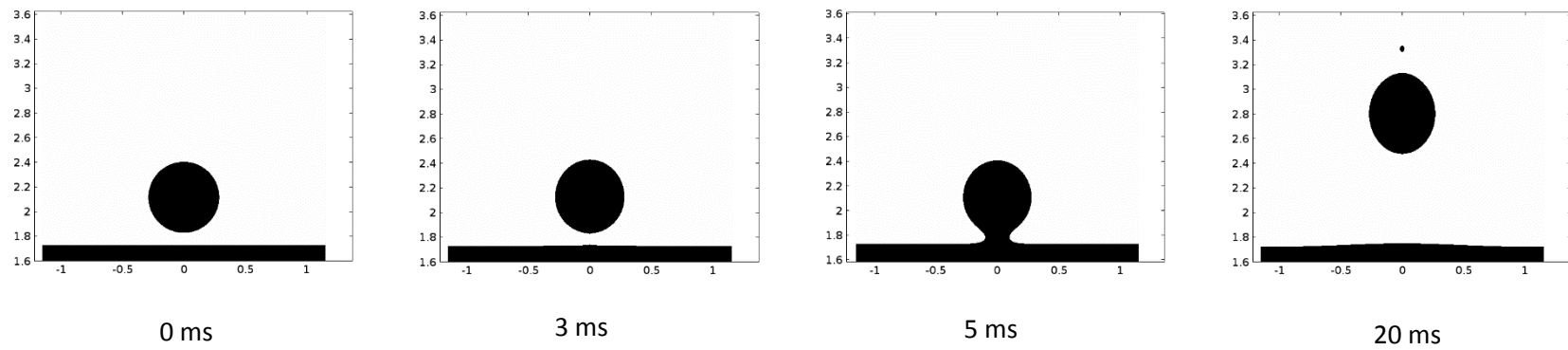


**Figure 7:** Calculated volume of secondary droplet formed as a function of the initial drop size for the system with properties reported in Table 2 and model parameters in Table 3.



(a)



(b)

**Figure 8:** Time evolution of drop-interface coalescence. (a) Complete coalescence, 0.08 mm initial drop-interface.

(b) Non-coalescence, 0.1 mm initial drop-interface distance.

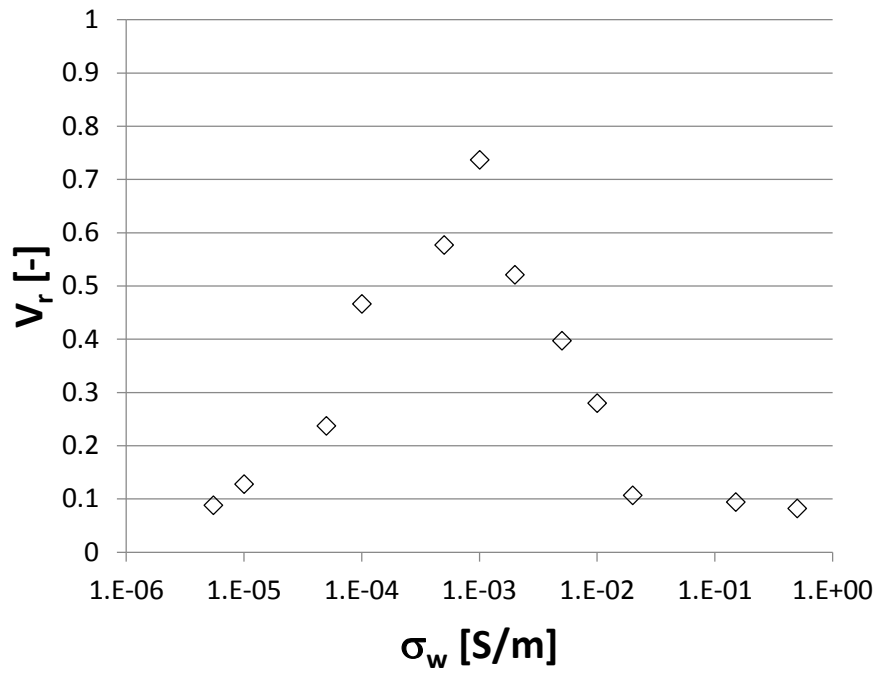


**Figure 9:** Calculated volume of secondary droplet formed as a function of the water conductivity for system with properties reported in Table 2.  $D=1.196$  mm,  $\xi/D=0.03$ ,  $h_{\max}/D=0.03$ .

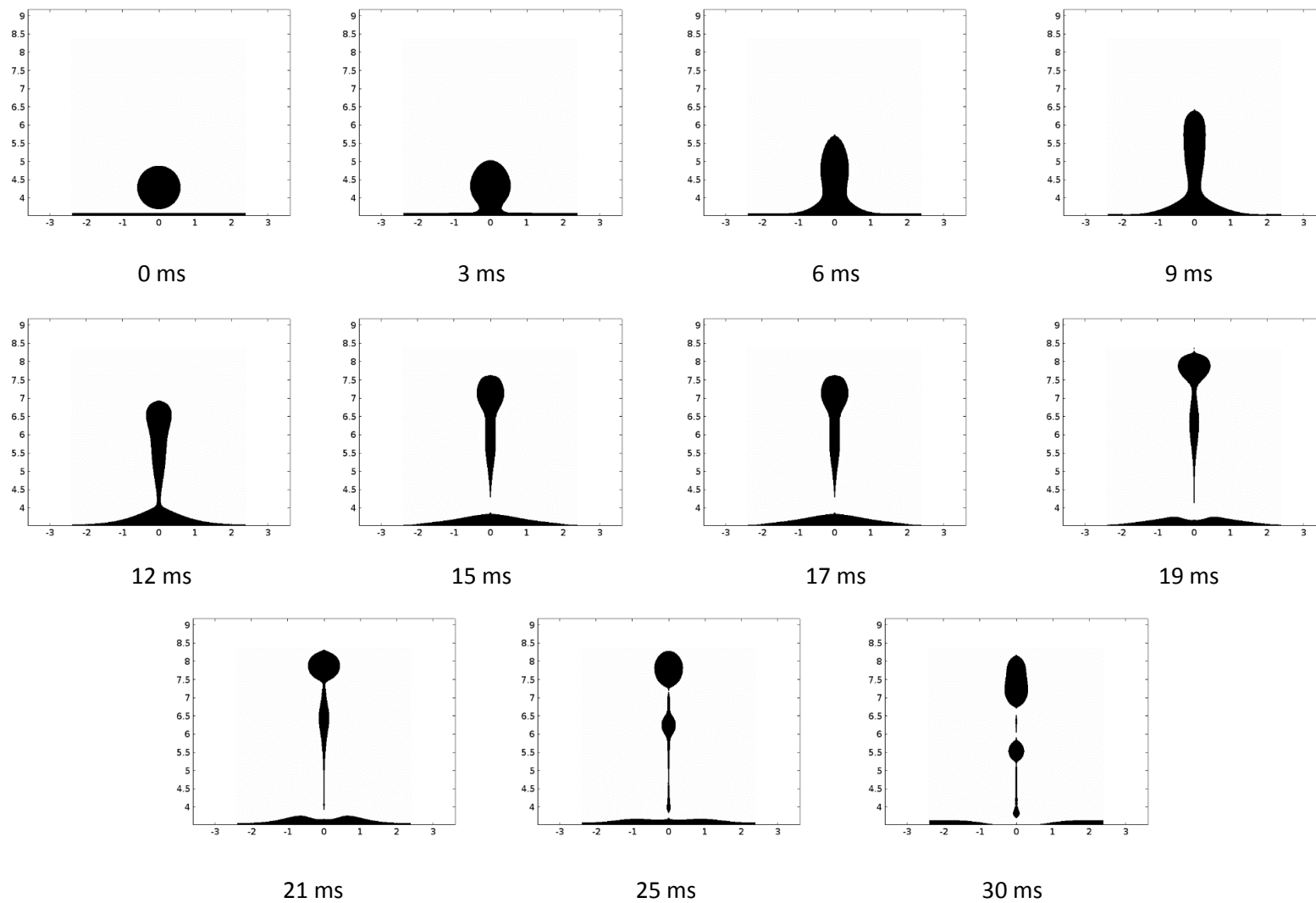


**Figure 10:** Time evolution of drop-interface coalescence:  $\xi/D=0.05$ ,  $h_{\max}/D=0.03$ ,  $\lambda=1 \times \text{m s}^{-1}$ ,  $D = 1.196 \text{ mm}$ ,  $\sigma_w = 10^{-3} \text{ S/m}$ .

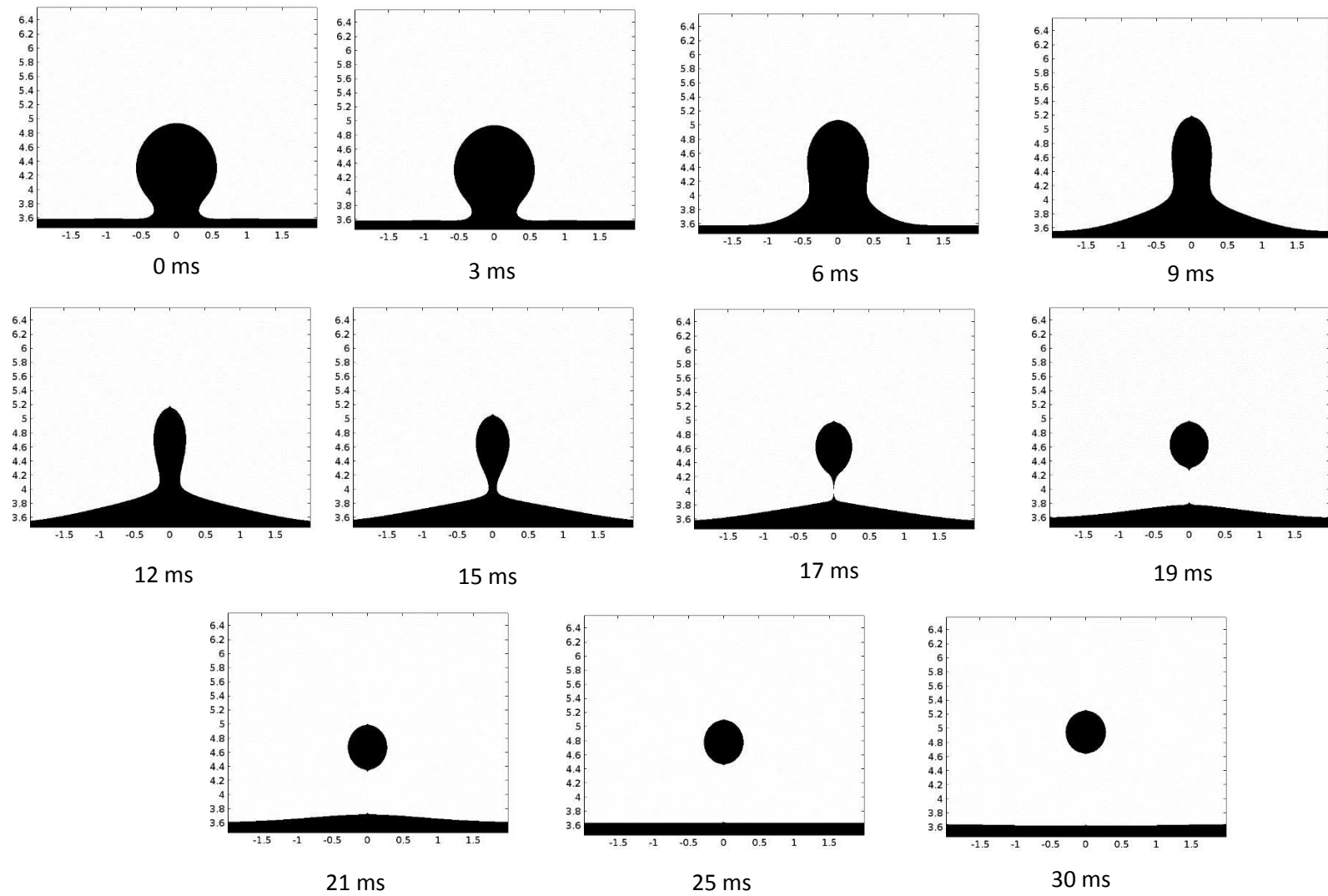


**Figure 11:** Time evolution of drop-interface coalescence:  $\xi/D=0.05$ ,  $h_{\max}/D=0.03$ ,  $\lambda=1 \text{ m}\times\text{s}^{-1}$ ,  $D = 1.196 \text{ mm}$ ,  $\sigma_w = 2\times 10^{-2} \text{ S/m}$ .

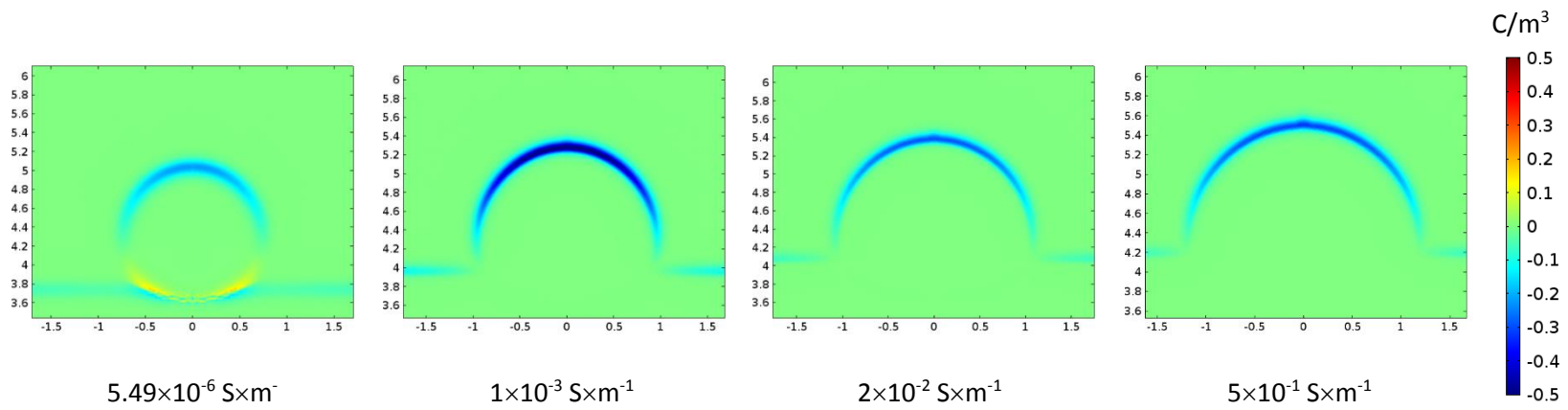


**Figure 12:** Space charge density ( $\text{C}/\text{m}^3$ ) in the coalescence region after 2 ms as a function of water conductivity.

**Table 1:** Properties of the experimental liquids (after Mousavichoubeh *et al.*, 2011b).

Liquid	Conductivity $\mu\text{S m}^{-1} (\pm 5\%)$	Viscosity mPa s	Density $\text{kg m}^{-3}$	Dielectric constant -
Distilled water	5.49	1.00	1000	80
Sunflower oil	$7.62 \times 10^{-5}$	46.5	922	4.9

**Table 2:** Effect of the interface thickness and maximum element size on the calculation results for the base case (NC: not converged).

$h_{\max}/D$	Volume of secondary droplets $V_r/\text{Initial Drop Volume}$		
	$\xi/D$		
	0.05	0.03	0.02
0.1	0	0.023	NC
0.05	0.0055	0.096	NC
0.03	0.084	0.088	0.144
0.02	0.082	0.086	NC

**Table 3:** Model parameters for the calculations shown in Figure 6.

Drop size mm	$\xi/D$ -	$\lambda$ m/s	$h_{\max}/D$ -
0.576	0.03	0.6	0.03
0.829	0.02	0.6	0.03
0.984	0.03	0.5	0.03
1.1	0.03	0.6	0.03
1.196	0.03	0.6	0.03

